5

DEEP ERT/IP for geothermal exploration and de-risking

A. Rosselli, C. Truffert, F. Barsuglia, F. Fischanger, A. Coletti, G. Morelli and S. Del Ghianda

5.1 Context

In a context of energy transition to limit greenhouse gas emissions, which have a deleterious effect on the climate, geothermal energy is playing an important role on the energy scene. After decades of development, operating technologies are now well mastered. However, one of the main obstacles to the development of this sector remains the investment cost, which can be broken down into several phases, including the discovery of a sufficient and sustainable thermal resource, the installation of the production plant, and its monitoring and maintenance. Locating a suitable and sustainable source of heat in the subsoil involves a high degree of geological risk and uncertainty. Geological risk, i.e. the risk of incorrectly positioning a borehole due to a lack of information about the subsoil and its properties, can be reduced by geophysical surveys that are suitably selected according to the geological context

DOI: https://doi.org/10.1051/978-2-7598-3752-6.c005

and the depth of the target. The resource exploration phase and in particular that which leads to the selection of drilling targets, the estimation of the resource volume and its future performance, conditions investors' decision-making. The key challenge is to maximize the probability of a project's success.

This document focuses on the upstream phase, resource exploration and in particular the use of geophysics to limit costs at 1 km depth maximum. This depth is well suited to a few medium-sized enthalpy projects, offering operators a favorable depth/temperature combination for heating or cooling installations, depending on the season. In specific geological contexts, these depths may also be compatible with power-generating geothermal plants.

5.2 Why electrical resistivity tomography is useful?

Electrical Resistivity Tomography (ERT) is a rather low-cost geophysical method, even when it comes to obtaining a three-dimensional image of the subsurface. The method highlights the electrical conductivity of the different parts of the subsoil. Over and above the intrinsic properties of geological formations, it is sensitive to weathering processes, water content and temperature. It has proved its worth not only in tabular geological environments, but also in geological systems with more complex geometries.

5.3 Deep electrical resistivity tomography for geothermal exploration – an Italian example

This article describes an example of a geophysical campaign performed by GEG Experts in Central Italy, in particular a Deep Electrical Resistivity Tomography (DERT) campaign, the aim of which is to gain a better understanding of the subsoil in order to assist operators of the medium-depth geothermal resource, while taking care not to disturb the upper aquifer.

The shallow aquifer, located around 300 m from the surface, is used to capture freshwater for domestic use. The deeper aquifer is potentially saturated in hypothermal water (temperature between 20 and 30 °C) or thermal water (temperature between 30 and 40 °C).

The initial ambition was to have a better knowledge over 1 km^2, at a maximum depth of 800 m.

The geology of the area under investigation bears witness to two distinct stratigraphic cycles. The first, of early-middle Pliocene age, is characterized by marine facies deposits. The second is marked by a phase of intense alteration, manifested in the form of brackish facies of age early Pleistocene.

An extensive debris layer has also been recognized, deriving from the intense weathering of oldest geological formations. This referred to the Riss-Wurm interglacial about 100 thousand years ago.

5.3.1 *Unconventional ERT data acquisition*

The survey is characterized by its significant extension and the required high investigation depth for ERT method. Moreover, the area is characterized by a typical hilly environment, with forests, roads and isolated houses or dispersed hamlets.

Given both these geographical constraints and the high depth of investigation, we considered that a traditional multi-electrode approach, using a conventional resistivity meter connected to multicore cables, would be unrealistic. Investigating at great depth requires an acquisition system that covers a very large area, which is incompatible with the geographical constraints mentioned above.

The acquisition system consists of a set of independent, stand-alone units, which record the variation in electrical potential over time on two measurement channels. The set of recorders is independent of the high-power underground current injection device. The current transmitter is powered by a generator and connected to a current recorder over time. The only cables running through the study area are those connecting the current electrodes to the transmitter. These are two small-section cables, far different from the multiwire cables used for traditional resistivimeter.

In particular, for this project, the configuration described below was used.

Receiver devices. The receiver system consists of 34 small and lightweight receiver boxes[2] that were easily deployed on the ground. Each box is independent and autonomous, powered by an internal battery, and allows electrical potential measurements to be performed at two dipoles: P1-P2 and P2-P3 (see Figure 5.1).

Each unit is therefore able to work independently from the others and this allows an “unconventional” 3D acquisition design in such a complex morphologically and logistically context. The receiver is able to continuously measure the electrical potential at the two dipoles with a frequency of 100 measurements per second. Its internal GPS device allows its localization and the timestamp for each measurement. The potential measurements are synchronized a posteriori with the current measurements recorded at the transmitter.

2. V-FullWaver from IRIS Instruments.

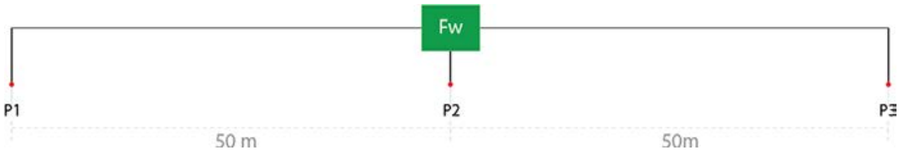

Figure 5.1 *Typical configuration of a recording unit used in this study. Three electrodes (P1, P2 and P3) are arranged for setting up two dipoles (P1-P2 and P2-P3). These dipoles could be either in the same direction (electrodes set up in-line as displayed on this figure) or perpendicular.*

Transmitter device. A high power current transmitter[3], specially designed for deep resistivity investigations, was used. It allows of handling a power up to 6 kW and injecting up to 16 A and 3000 V into the ground. The transmitter was powered by a large dedicated three-phase 15 kVA motor generator (see Figure 5.2). The "automatic range" mode allows the optimal injection level to be automatically selected according to the contact resistances at the TX-A and TX-B electrodes. The current is injected into the ground according to a 2 sec IAB+, 2 sec OFF, 2 sec IAB-, 2 sec OFF scheme and is recorded every 10 ms by means of an current recorded box. Thanks to its internal GPS, the current is also timestamped. This allows, as already mentioned, the retrospective synchronization of all potential signals (Vmn) recorded together with the injected electric current (Iab).

Figure 5.2 *On the left, high power transmitter of 6 kW. On the right, the three-phase 15 kVA motor generator which powers the transmitter.*

3. TIP6000 from IRIS Instruments.

Topography – For an ERT survey, accurate location of the receiving and injection electrodes is essential. The position of each electrode was measured by a DGPS Leica GS18 system with an accuracy of less than 3 cm.

A digital Lidar terrain model with a 2 m×2 m mesh was used to build a detailed 3D finite element mesh for the ultimate phases of data processing.

5.3.2 *Acquisition methodology*

The implementation of a DERT project on the ground can be divided into 4 fundamental phases: survey design, field preparation, data acquisition and equipment recovery.

The survey design is a step done at the office that must not be neglected. Backed in part by logistical issues, it contributes to the optimization of human resources, intervention time and data quality. A detailed study of the area based on aerial photos, topographic map and direct inspections allowed to identify the access routes, the ideal position for the receiving units and transmissions electrodes. Using our proprietary ERTdesign© software (GEG Experts), we generated an initial theoretical layout of receivers and transmissions over the study area (see Figure 5.3). We then optimized the results by accurately moving each receiver or transmission point based on consideration as access or visibility of satellite constellations to ensure a good GPS connection.

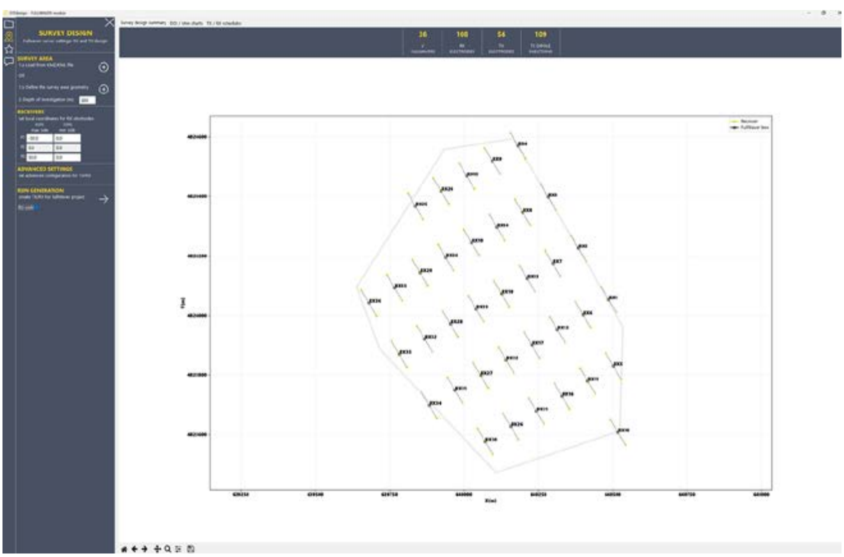

Figure 5.3 *Acquisition design performed before the survey with ERTdesign©. The software provides the total number of receiver units (displayed on the figure) and transmission points.*

The *survey design* phase is followed by the subsequent *field preparation*. It took one day to indicate on the field the future location of injection and receiving electrodes using a wooden sticks. This helps the subsequent deployment of the units and avoid any error (Figure 5.4).

Figure 5.4 *Receiver box deployed at the wooden stick location.*

The *data acquisition* campaign was completed in 2 days, including *retrieval of equipment*, by a team of 12 people, adequately trained.

5.3.3 *Acquisition layout*

The acquisition was carried out by arranging the receiving (green) and transmitting (red) electrodes according to the design shown in Figure 5.5.

The survey involved the arrangement of a 5.5 km long central transmission axe (from TX1 to TX23, in yellow in Figure 5.5), necessary to be able to achieve a depth of 800-900 meters. Other injection dipoles are positioned in the area of interest. These smaller dipoles (in white), located close to the receiver units (green dots), are designed to improve near-surface resolution.

The field team deployed 34 reception boxes each one connected to three electrodes (in detail in Figure 5.6) according to the design previously described. The size of each receiving dipoles is 50 meters (P1-P2 = 50 m, P2-P3 = 50m). A total of 102 receiving electrodes has been set up.

Figure 5.5 *Aerial view of transmissions points (in red) and receivers points (in green). The longest distance on injection dipole along the main axe (in yellow, between TX1 and TX 23) is about 5.5 km. The white lines, more central on the figure, show the cables used for shorter distance transmissions, inside the area of interest.*

Figure 5.6 *Layout of 102 electrodes and 34 recording units in the area of interest.*

5.3.4 *Current transmissions*

The transmissions have been designed according to two approaches, based on the dual need to reach deep layers and, at the same time, to have a fair near surface detail.

A first series of 32 transmissions was carried out with the aim of achieving the maximum sensitivity of the measurements at great depths for the different receivers.

For these currents' injections, a fixed pole "A" in TX1 and a second mobile transmitter "B" with a "forward" acquisition scheme was used: TX1-2, TX1-3, TX1-4, ..., TX1-23 (Figure 5.7). The injection dipole TX1-23 has the maximum aperture of about 5.5 km.

Figure 5.7 *Location of the transmission's electrodes on main central axe. Pole A was in TX1 and pole B was moving on all TX from TX2 to TX23. A backward acquisition was done on the main axe, with pole A fixed at TX23 and pole B moving backward on TX21, TX19, TX17, …, TX1 (one out of two).*

This acquisition sequence was followed by a backward energization scheme with fixed pole "A" in TX23: TX 23-21, TX23-19, TX23-17, ..., TX23-1 (Figure 5.7). The combination of these transmission dipoles schemes allowed to acquire (i) dipole-dipole protocol arrays, when the transmitting dipole is very far from the receiving dipole, (ii) pole-dipole, when the mobile transmitter "B" is close to the receiving dipole, and, (iii) gradient dipole, when both transmitters "A" and "B" are "external" and far from the receiving dipole.

The second group of transmissions (72 dipole combinations) involved electrodes with numbering from TX24 to TX50, each of which has been combined in sequence with three different "remote" transmission poles, fixed respectively at the TX9, TX13 and TX15 electrodes (Figure 5.8). This approach enabled us to achieve high-sensitivity measurements across the area of receivers, effectively covering both shallow and medium investigation depths.

Figure 5.8 *Close up view of Figure 5.5 showing transmissions performed in the zone of interest. Pole A was alternatively placed at TX9, TX13 and TX15, while pole B was moving on TX24 to TX50.*

5.3.5 *Quality control*

With regard to chargeability data (induced polarization), which the receiving system and injection protocol enable to acquire in an auxiliary manner, measurements are of good quality at the first 350 to 400 meters. For deeper measurements, characterized by low-intensity electrical potential signals, the potential discharge curves do not allow this information to be extracted. Figure 5.9 shows the details of the signal recorded at the first channel of the RX3 receiver at the transmission event between the TX1 and TX2 electrodes, the smallest dipole of the main transmission axe. This demonstrates how the receiver effectively detects the subtle signal from the electric field generated by the transmission dipole, even over a significant distance between the injection point and the receiver. The presence of about 40 measuring stacks, recorded during almost 3 minutes of current injection, allows us to identify a very good average signal (graph at the bottom left in Figure 5.9), with an amplitude of the order of 0.04 mV. The chargeability measurements (graph at the bottom right) are of mediocre quality, with potential discharge curves that are difficult to identify.

Figure 5.10 displays the same type of graphs, in the more favorable situation of the TX15-13 transmission dipole recorded by the first channel of receiver no. 16. Note that in this case, by virtue of the higher V signal (about 12 mV), the discharge curve and the consequent derivation of the chargeability measurement is more robust.

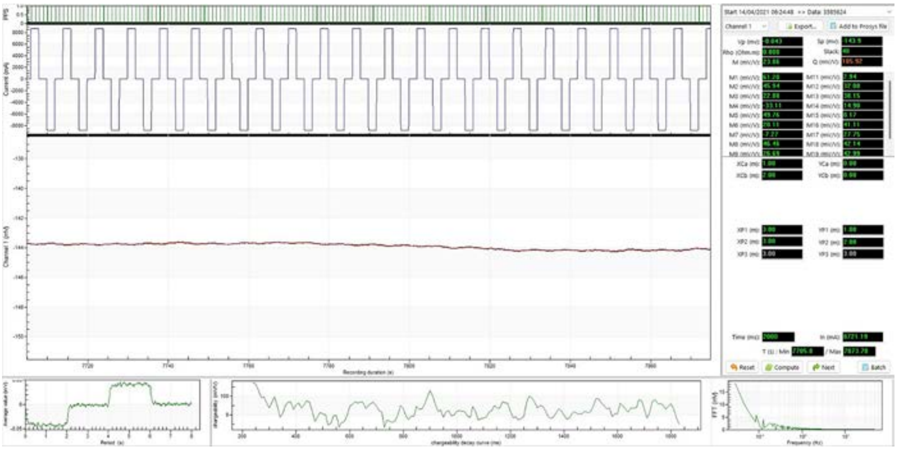

Figure 5.9 *In blue the graph of the time trend of the current intensity (mA) injected at the TX1-TX2 transmission dipole (about 8720 mA). In red is the graph of the time trend of the corresponding signal V(mV) recorded by the first channel of the receiver box no. 3. At the bottom left the signal averaged on the different measurement stacks. At the bottom right the chargeability discharge curve.*

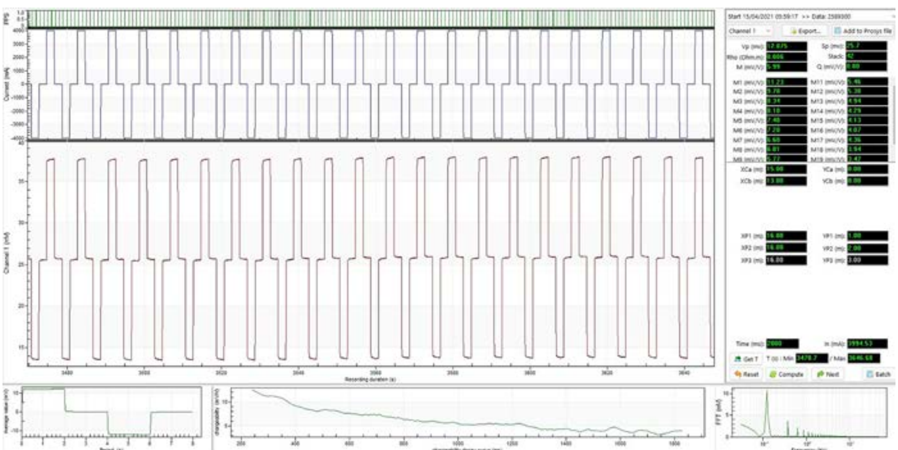

Figure 5.10 *In blue the graph of the time trend of the current intensity (mA) injected at the TX15-TX13 transmission dipole (about 4000 mA). In red is the graph of the time trend of the corresponding signal V(mV) recorded by the first channel of the receiver box no. 16. At the bottom left the signal averaged on the different measurement stacks. At the bottom right is the chargeability discharge curve.*

In statistical terms, the I_{AB} currents transmitted during the three days of acquisition are on average of the order of 4.5 A, with minimum values of 3.2 A and peaks of 8.8 A, reached with transmissions in the South-East area on more conductive soils. The average Vmn potentials recorded are of the order of 3 mV, with average apparent resistivities around 20 Ω·m, with the lowest values, around 8–10 Ω·m, measured at depth (Figure 5.11).

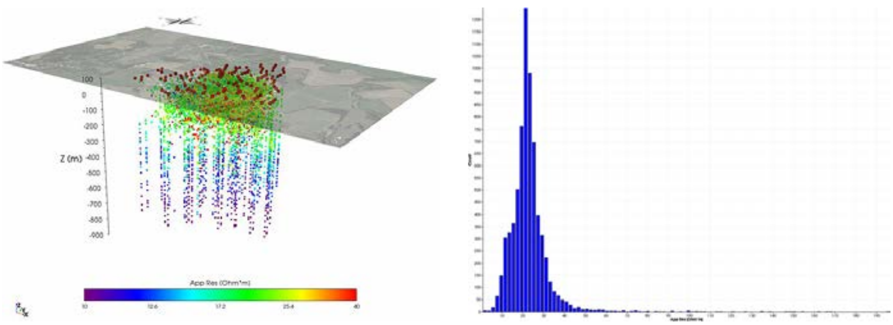

Figure 5.11 *Pseudo-cloud of measured apparent resistivities (on the left) and histogram of measured apparent resistivities (on the right).*

The cloud of the measured apparent resistivities is displayed on Figure 5.11 (left). The total set of measurements consists of 7072 quadripoles (104 transmissions for 68 receiving dipoles). Before the resistivity measurements were processed from the global set, 147 measurements, equal to about 2%, were removed. Most of them had measured Vmn signal less than 0.01 mV.

For the processing of the chargeability measurements, we opted for an arithmetic sampling of the discharge curve, using a delay time of 240 ms and 20 sampling windows of 80 ms. After resistivity inversion, we filtered the chargeability measurements, excluding data with a standard deviation above 10% and IP values outside the 0.01–30 mV/V range. This filtering removed approximately 2500 inaccurate measurements, representing about one-third of the dataset primarily associated with deeper quadripoles where the larger distance between receiver and transmitter resulted in lower potentials (below 0.5–1 mV). The inverted dataset showed average chargeability values around 5 mV/V.

5.3.6 *Processing of resistivity and chargeability measurements*

The investigation enables us to reconstruct three-dimensional models of the distribution of resistivity and electrical chargeability of the subsoil, which highlight the main lithological characteristics of the site. The geological context is relatively conductive, with electrical parameters varying within the first 300–350 meters of depth. Low-resistivity formations, such as clays and silts, surround zones of higher resistivity (up to a few tens of Ω·m), which may correspond to sandier layers and thus indicate potential aquifer formations. Below 300-350 meters, the geological formations exhibit high conductivity with resistivity values around 10 Ω·m, continuing uninterrupted down to the survey's lower limit at 800–850 meters (see Figure 5.12).

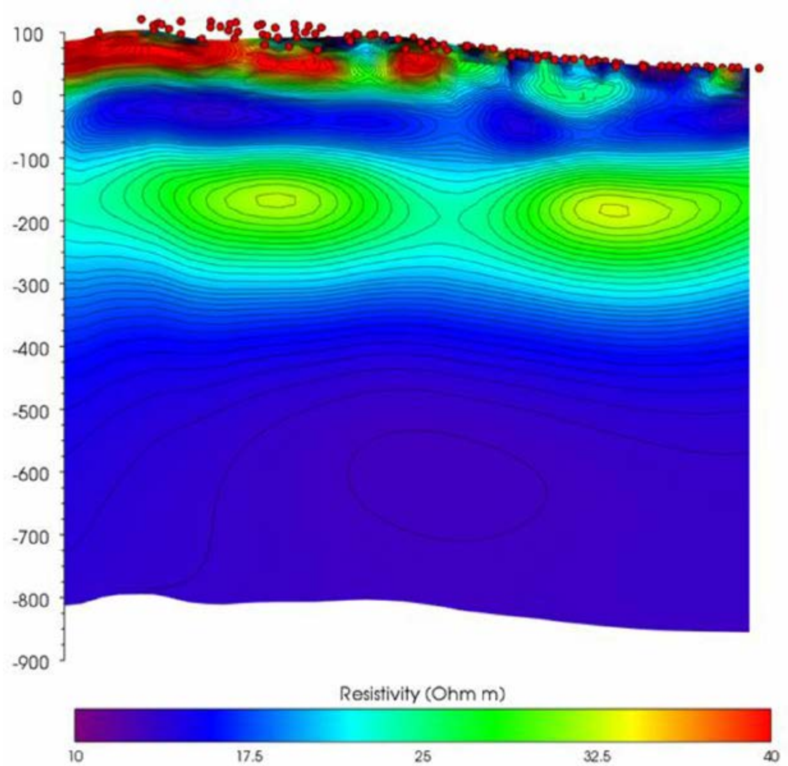

Figure 5.12 *Resistivity section.*

The ERT measurements were inverted using the ERTLab Studio software, following the removal of inaccurate measurements as outlined in the previous section. The three-dimensional inversion was conducted with the following configuration:

1. implementation of the complete topographic model,
2. mesh size 25 m×25 m×12.5 m in the x, y, and z directions of space,
3. depth of investigation equal to 900 meters from ground level,
4. initial resistivity inversion model set to of 15 Ω·m, corresponding to the median of apparent resistivities values,

5. starting model for 5 mV/V chargeability inversion,
6. estimated data noise of 1.5% for resistivity processing and 5% for IP data processing.

The resistivity and chargeability inversions both converged, respectively in 6 and 4 iterations, with an excellent concordance of the modeled measurements with respect to the site acquisitions. This is illustrated on the examples in Figure 5.13, showing the cross-plot of the measured data compared to the modeled data at the end of the inversions.

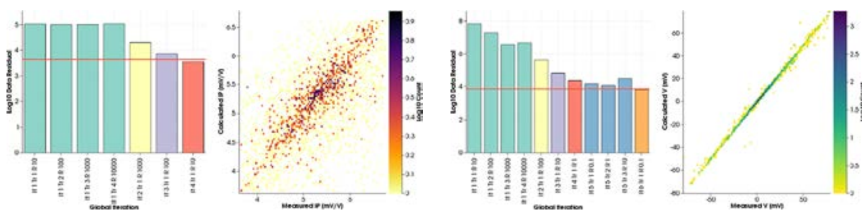

Figure 5.13 *Graphs of resistivity inversion progress. Left: trend of the measure-data misfit modeled as the iterations progress. Right: cross-plot of modeled data vs. measured data at the end of the inversion.*

5.3.7 ***Results***

This 3D Deep Electrical Resistivity Tomography approach allowed to highlight potentially aquifer sandy portions within the first 250–300 meters from the ground level. Figure 5.14 shows the geological map of the investigated area as well as a schematic geological section of the same area. These potential sandy portions are characterized by electrical resistivity values around 20–30 Ω·m and represented by a red-orange color Figure 5.15. The aquifer is well known from existing boreholes in the same region and is related to a fine sands layer (P3 in Figure 5.16). It is confined at the top by a more conductive layer related to sandy clays (Q1 in Figure 5.16).

With regard to investigations for the deep geothermal aquifer, the 3D model shows the presence of zones with very low electrical resistivity (<20 Ω·m) starting from 300–350 m below sea level down to the base of the investigated volume. These more conductive zone can be interpreted as related with the blue clays layer (P in Figure 5.16 and 5.14).

We notice that within the conductive layer we can isolate a plume characterized by even lower resistivity values, below 12 Ω·m (A, Figure 5.16).

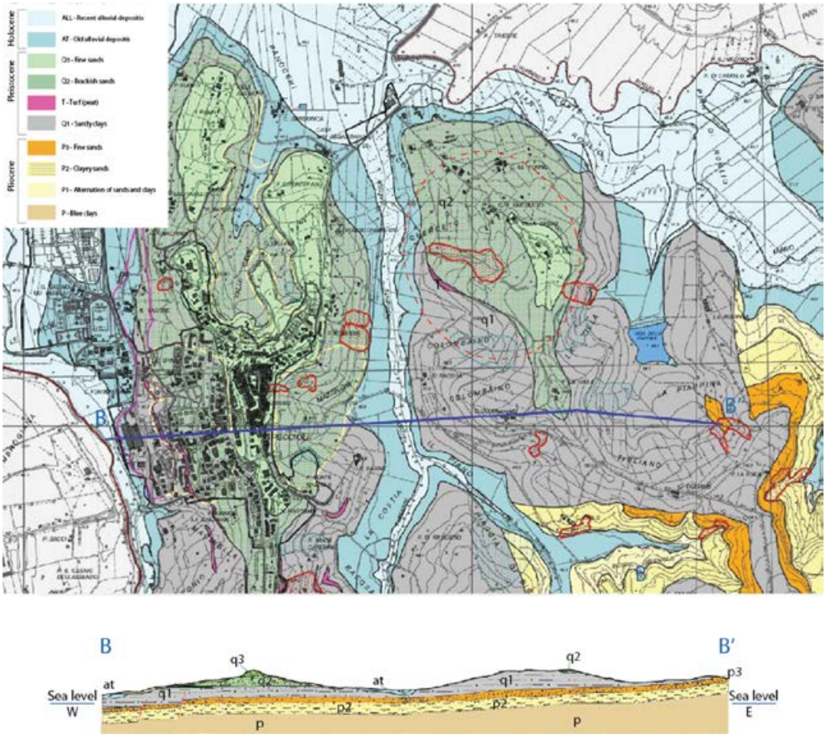

Figure 5.14 *Geological map of the investigated area (red circle) and geological section.*

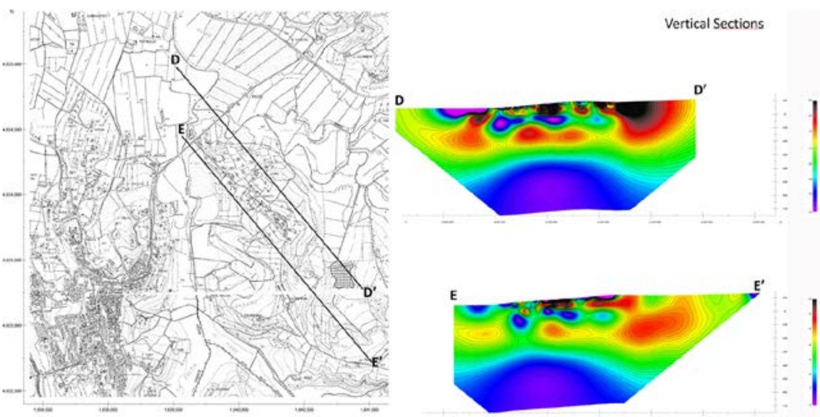

Figure 5.15 *The vertical sections issued from the 3D resistivity model show the presence of a possible shallow aquifer (sandy layer) at an altitude of about 150 m below sea level (red-orange color) and a possible thermal reservoir at the altitude of about 350 m below sea level (blue/purple color).*

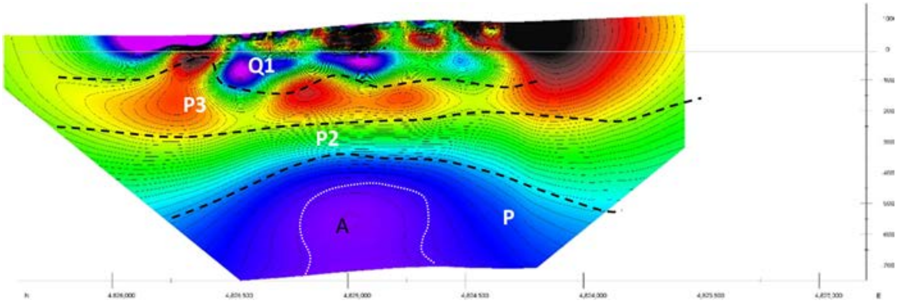

Figure 5.16 *Geological interpretation of the 3D ERT model.*

The Induced Polarization, despite an extremely heterogeneous chargeability in the first 200 m below the surface that partially hides the deeper signal, shows a very interesting correlation between a deep low chargeability zone (B Figure 5.17) and the conductive plume at about 500 m below sea level.

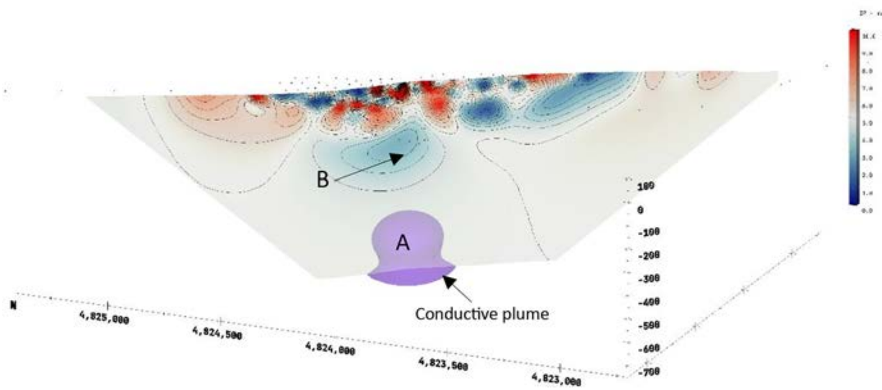

Figure 5.17 *IP section with high conductive plume.*

The analysis of both resistivity (rho) and chargeability (IP) results suggest that the high conductivity of the deeper layer (A, Figures 5.16 and 5.17) associated with the presence of a low chargeability area (B, Figure 5.17) could be interpretated as being linked to deeper fluids at higher temperatures. This is compatible with the presence of a low-enthalpy geothermal system.

Conclusion

ERT is one of the geophysical techniques both sensitive to water content and temperature. Traditional ERT equipment, known as resistivimeters, combining a central instrument that controls current injection and potential measurements, remain highly effective for obtaining high-resolution knowledge of conductivity distribution in the ground. However, the depth of investigation is not compatible with the demands of geothermal energy. The use of recording units separated from high-power transmitters for deep investigation is more appropriate. Unfortunately, this requires the management of long reception cables in the field, which is very laborious and can generate strong coupling effects that are problematic for the final quality of the data.

Thanks to the use of self-contained receivers, deep 3D field surveys are accessible to organized and meticulous field operators. The cost of this type of survey, provided the team is experienced, remains very low when compared with other geophysical techniques or with poorly positioned drilling. ERT alone cannot guarantee geothermal drilling, but when combined with geological knowledge, it can guide the man of the art in his interpretation. These new acquisition systems and protocols pave the way for wider use of ERT in medium-depth geothermal energy.